

Research Article

Underwater Image Restoration Using In-situ Turbidity Measurements

Irmiya R. Inniyaka¹, Yuya Nishida², Kazuo Ishii²

¹Department of Life Sciences and Systems Engineering, Kyushu Institute of Technology, 2-4 Hibikino, Wakamatsu, Kitakyushu, Fukuoka 808-0196, Japan

²Department of Human Intelligent System, Kyushu Institute of Technology, 2-4 Hibikino, Wakamatsu, Kitakyushu, Fukuoka 808-0196, Japan

ARTICLE INFO

Article History

Received 11 November 2022

Accepted 15 October 2023

Keywords

Underwater image restoration

Turbidity

Attenuation coefficient

Beer-Lambert law

ABSTRACT

Degradation in underwater imaging is as a result of absorption and scattering of light. Propagated visible light rays through the water column are absorbed at rates that vary depending on the wavelength of light. Large suspended particles also scatter the propagated light rays, as can be observed in an underwater environment. Furthermore, color is distorted due to the inverse ratio of attenuation that is proportional to the wavelength of light through a unit of length through the water column. These phenomena distort underwater images by making them appear dark and have low contrast. Conventional underwater image restoration techniques are largely based on the image formation model (IMF) which restores the image based on estimates from the degraded images. The results are solutions that are limited to specific underwater conditions. In this paper, we propose a novel restoration strategy by considering the optical properties in the underwater environment at the time of image capture, a robust restoration technique can be applied to images captured in different underwater conditions. In so doing, we design a turbidity meter that capture wavelength-dependent absorption data which are applied as parameters to restore the distorted images based on the RGB channels. To validate our proposed technique, we conduct experiments in a controlled underwater environment while varying the concentration of suspended particles based on degree of kaolin mixture.

© 2022 The Author. Published by Sugisaka Masanori at ALife Robotics Corporation Ltd.
This is an open access article distributed under the CC BY-NC 4.0 license
(<http://creativecommons.org/licenses/by-nc/4.0/>).

1. Introduction

1.1. Overview

Imaging in the underwater environment has become an important aspect of interest for many branches of scientific research and technology. This is due to its influence for target goals like; successful control of underwater vehicles, inspection of man-made underwater infrastructure, cables and objects, marine biology research, and archeology. Contrary to terrestrial imaging which are clear, capturing images underwater is a challenging task which poses a negative impact to successful performance of robotic systems in underwater operation [1], [2], [3].

1.2. Underwater imaging

Underwater images suffer degradation in contrast and color distortion primarily due to the interaction of light while propagating through the water medium. From the illustration portrayed [Figure 1](#), travelling rays of light from a light source to the target scene is influenced in 2 ways. Firstly, the intensity of the light is attenuated with increasing depth through the water column. The attenuated light is dependent on individual wavelength where longer wavelengths attenuates faster than shorter wavelengths. We see that the red wavelength totally attenuates at about 5[m] depth while the wavelength of blue light can reach 60[m] water depth. This is the

Corresponding author's E-mail: irmiya.inniyaka-reuben350@mail.kyutech.jp, y-nishida@brain.kyutech.ac.jp, ishii@brain.kyutech.ac.jp
URL: <https://www.kyutech.ac.jp>

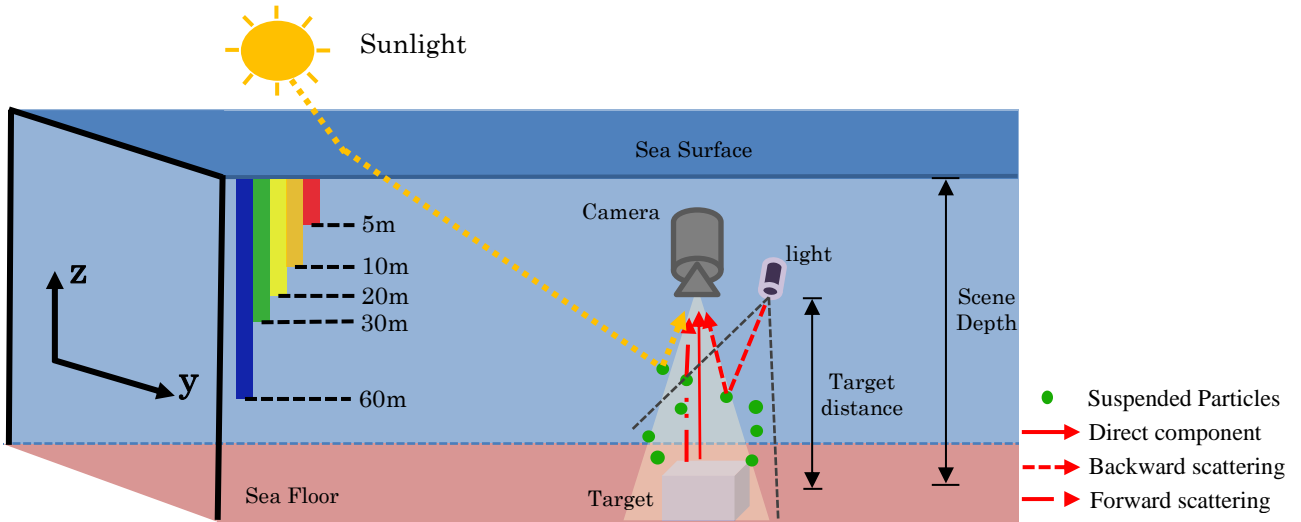


Figure 1: Underwater Imaging Model

phenomena that causes underwater images to appear bluish.

In the second scenario, propagated light rays collide with suspended particles in the underwater medium. This tends to alter their direction of propagation leading to a phenomenon called scattering. The scattering is either forward scattering (0° - 90°) or backward scattering (90° - 180°) [8]. The resultant effect is a blurry image with reduced contrast. And hence, the combined attenuation and scattering due to the inherent nature of how light interacts with the underwater environment leading to distorted imaging [2], [3].

2. Underwater image restoration

In proffering solutions to correct distorted underwater images, researchers have developed numerous underwater image restoration techniques. Conventionally, restoration techniques are based on the hazy atmospheric image model proposed by McCartney in 1976 [6], [7], [8] as represented in Eq. (1). It is also commonly referred as the Image Formation Model (IFM).

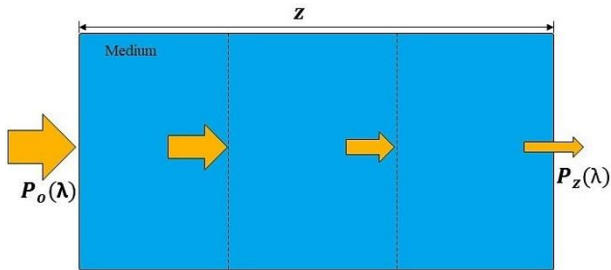


Figure 2: Attenuation of Light in Water

While the application of this model proves successful in some underwater conditions, its generalization ability is poor and hence will require parameter tuning to be suitable for different imaging conditions.

Another limitation of the Image formation model for underwater application is tied to the assumption that the coefficient of attenuation is constant. In restoration of hazy images taken in the atmosphere, attenuation of light is assumed to be wavelength-independent. However, this is an ill-posed model for the underwater imaging where attenuation of light is wavelength-dependent. As such using the image formation model for restoring underwater images will be insufficient not only because attenuation if light is wavelength-dependent but also because attenuation parameters change with climate, geography, season, and water type [4], [8]. Hence, applicable use of IFM for underwater images, requires color channel-based image restoration. The digital imaging color channels are red, green and blue (RGB). This approach further gives rise to more unknown values as opposed to IFM application for terrestrial imaging.

Previous proposed techniques, estimate these unknown values from the captured underwater image using different approaches. This estimation method proves insufficient to meet the varying nature of imaging underwater. We propose that by providing actual measurements to the formation model, a robust and improved restoration can be achieved. In this paper, we propose that by measuring the optical variation as it affects light transmission for each of the three channel of light we can improve the restoration ability. In doing so

we design and develop an optical sensing unit (turbidity meter) for real-time measurement of turbidity as a means of applying wavelength-dependent attenuation coefficient to restore degraded images. The paper is further organized into the following sections. In [Section 2](#), the design principle and structure of the turbidity meter is described. [Section 3](#) presents the hardware structure and [Section 4](#) describes the experimental setup and result discussion. The conclusion and future task to be conducted are presented in [Section 5](#).

3. Design Principle

3.1. Underwater Image Restoration Based on IFM

Applying the IFM for underwater correction is carried out on each respective color channel as represented by lambda in [Eq. \(1\)](#); $\lambda \in \{R, G, B\}$. An Images' intensity at each pixel comprises of 2 components, the direct signal which has been attenuated and backscattered component as shown in [Eq. \(1\)](#) [3], [4], [9].

$$I_{k,\lambda}(x) = I_{0,\lambda}(x) \cdot t_{k,\lambda}(x) + (1 - t_{k,\lambda}(x)) \cdot A_{k,\lambda}(x) \quad (1)$$

From [Eq. \(1\)](#), $I_{k,\lambda}$ represents distorted image captured at the camera, k is the concentration of suspended particles in the water medium when image is captured, x is the pixel coordinate of the image, $I_{0,\lambda}$ represents the clear image or scene radiance we desire to recover ($k = 0$ for this image), $t_{k,\lambda}$ is the transmission per color channel and $A_{k,\lambda}$ is the homogenous global veiling light. The transmission [Eq. \(2\)](#) depends on the target-object distance $z(x)$ in the scene and decadic absorbance coefficient α_λ [15] for each color channel:

$$t_\lambda = \exp(-\alpha_\lambda z(x)) \quad (2)$$

Contrary to terrestrial image restoration which assumes a constant coefficient of attenuation per color channel, in this work we aim to influence of wavelength-dependent attenuation β_λ by varying the concentration of suspended particles in the water medium and simultaneously taking the turbidity measurement/capturing the image for each scenario. We use the transmission of light method to determine the attenuation. The total attenuation coefficient β_λ describes how much the rays of a light for a particular wavelength is attenuated over travel distance through the medium. As postulated in Bouguer-Beer-Lambert law,

“the intensity of light decreases exponentially with distance. The formulation is as expressed in [Eq. \(3\)](#) and [\(4\)](#):

$$A = \log\left(\frac{P_0}{P_z}\right) \quad (3)$$

$$\beta = \frac{1}{z} \log\left(\frac{P_0}{P_z}\right) \quad (4)$$

$$I_{0,\lambda}(x) = \frac{I_{k,\lambda}(x) + (1 - t_{k,\lambda}(x)) \cdot A_{k,\lambda}(x)}{t_{k,\lambda}(x)} \quad (5)$$

$$I_{0,\lambda}(x) = \frac{I_{k,\lambda}(x)}{t_{k,\lambda}(x)} \quad (6)$$

From [Eq. \(3\)](#), A is the absorbance of light traveling a certain distance z from the source P_0 to the target scene distance P_z . The equation is rearranged to [Eq. \(4\)](#) where the distance of light travel by z is factored in to calculate the attenuation coefficient β . This is as described in [Figure 2](#) [13]. Therefore, to restore an underwater image [Eq. \(1\)](#) takes the form as written in [Eq. \(5\)](#) where $I_{0,\lambda}$ is the subject. However, in this study, the designed turbidity meter senses the absorbed intensity. Hence, the restoration equation takes the form of [Eq. \(6\)](#) where the backscattering parameter is ignored. This is a limitation of the turbidity metering design that will be addressed in subsequent study.

3.2. Turbidity (Sensor design principle)

Turbidity is a physical property as relates to the cloudiness or clarity of a water medium. It is an optical characteristic of water that is quantified by measuring the intensity of scattered light that is transmitted through the liquid medium due to collisions with suspended matter like silt, clay, algae, planktons, tiny organic and inorganic mater [10], [11], [12]. The higher the presence of suspended particles, the higher the cloudiness and degree scattering of transmitted light in the water body.

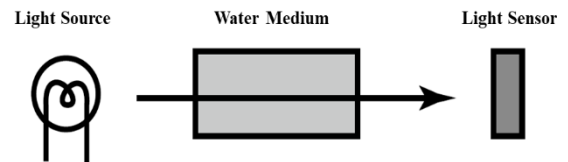


Figure 3: Transmitted Light method of turbidity measurement

In this work, we design a simple turbidity meter that operates by measuring the intensity of transmitted light when immersed in a water medium with varying concentration of suspended particles. Using the sensor

measurements, we calculate the attenuation coefficient for each scenario. The design solution is based on transmitted light as described in Figure 3 and stipulated by Japanese Industrial Standard (JIS) K0101 “Testing Methods for Industrial Water” in [5]. Basically, a constant light is transmitted over a preset distance from a light source point at one side of the water medium and is measured at the opposite side by a light sensor. Although the light at source is constant, the measured intensity varies when the concentration of suspended particles in the water medium is varied. The intensity variation is expected to vary for different wavelengths of light. In a

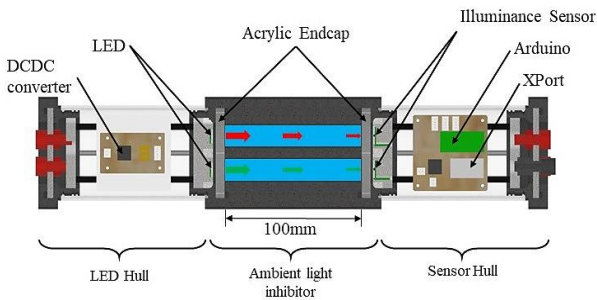


Figure 4: Cross-sectional view of Turbidity Meter

previous work [13], [14], the transmission of light method was used to determine absorbed light rays underwater for different degree of turbidity. The designed turbidity meter was deployed to for image restoration to detect cracks in underwater infrastructures. The results of image restoration were poor mainly due to the design of the turbidity meter. Only a single red LED was used as the light source for the design, this means that only one attenuation value was used for the 3-channels of underwater image correction.

To improve on this drawback, we propose a turbidity meter design that measures attenuation for each respective channel of the associated underwater image. In doing so, the turbidity meter is designed to satisfy the following requirements.

- A modular configuration for ease to mount on an underwater vehicle.
- Continuous data acquisition and transfer.
- Measure turbidity for the 3 color channels (RGB).
- Inhibit ambient illumination.

4. Hardware structure of turbidity meter

From the image depicted in Figure 4, the structure of the turbidity meter is cylindrical and designed to have 3 main parts; 3-inch acrylic LED hull, 3-inch acrylic sensor hull

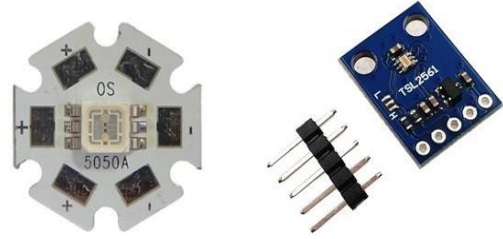


Figure 5: Power LED (left) and Light Sensor (right)

and ambient light inhibitor. It has a dimension of 480 x Φ 130 [mm] and weights 2.7kg in Air. The LED hull is composed of 3 LEDs (illuminating red, green and blue light respectively) positioned at 120° from each other and aligned to the 3 light sensors housed in the sensor hull. images of the LED and light sensor used are shown in Figure 5. The hulls are positioned at a distance of 100[mm] facing each other and held in place by the ambient light inhibitor. This distance is the optical path as recommended by JIS K0101. The ambient light inhibitor is a 3D printed polylactic acid (PLA) model that provides several functions. Inclusive of the aforementioned function it blocks out external light, restricts each light source to its light sensor, provide a path for water inlet and exit, and maintains a constant distance of transmitted light. Table 1 shows the specification of the turbidity meter.

Table 1: Turbidity Meter Component Specification

Category	Specification
Weight in Air	2.7kg
Illuminance Sensor	TSL2561 (0.1 – 40,000 lux)
Power LED [Red, Green, Blue]	RGBLED-OSTCWBTHC1S [624nm, 525nm, 460nm]
Power Supply	5V
Current	18mA
Microcomputer	Arduino Nano
Communication	I ² C, Ethernet, XPort

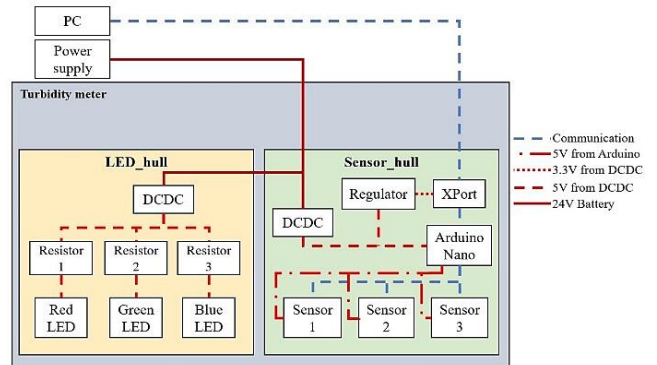


Figure 6: Overview of Electrical system

4.1. Overview of System Architecture

In this subsection, a brief description of the turbidity meter electrical and communication design is outlined. A diagrammatic representation is as shown in Figure 6. In the LED hull, a DCDC converter steps-down source voltage from a maximum of 24v to 5v. This is supplied to each LED through individual resistors that limit current supply to the rated current.

In the sensor hull, a DCDC converter also steps-down source voltage to 5v. The 5v powers an Arduino microcomputer and the light sensors but is also regulated to 3.3v to power the XPort device.

The turbidity meter communicates in 2 levels; between the light sensors and microcomputer communication is achieved via I²C, while the communication between the microcomputer and onboard PC uses and ethernet facilitated by an XPort module.

5. Experiments and Results

To evaluate the performance of turbidity measurement devices, Turbidity standard solutions are commonly used; such as the formazin, kaolin and polystyrene (PSL) standard solutions. In this work, experiments are conducted based on the kaolin standard solution. This is the standard for measuring turbidity according to the Japanese Industrial Standard. It is also safe for use, easily accessible and low-cost relative to the other standards.

5.1. Experiment I

In this experiment, an apparatus is constructed as shown in Figure 7. Using the setup, an assessment of light absorption in kaolin solution can be performed by varying 2 parameters in the experiment; the concentration of Kaolin solution and the water depth. The setup consists of a 3-inch cylindrical PVC pipe that prevents ambient light from penetration. The Sensor hull is mounted at the lower part of the pipe using a 3D printed jig to make the attachment rigid and watertight while the LED hull is mounted at the top side.

Differing lengths of PVC Pipes are prepared to simulate different water depth through which light travels. The PVC pipe lengths are 5, 10, 20, 30, 40, 50 and 60 [cm] respectively. The purpose of the experiment is aimed at generating absorption data of each LED as it travels through different water depth and in different concentration of the Kaolin solution. Hence, for each PVC pipe, the light is transmitted through Kaolin solution



Figure 7: Experimentation Setup

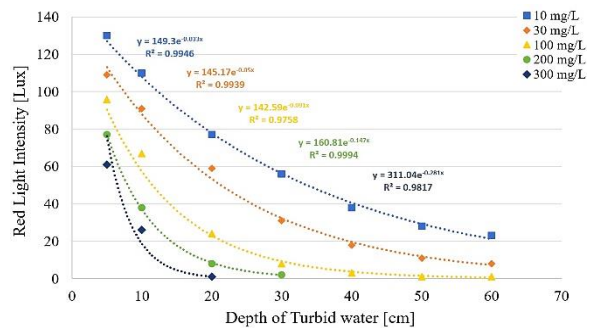


Figure 8: Red LEDs' absorption at different water depth

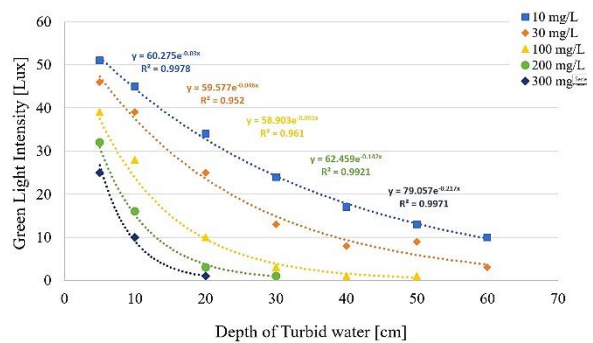


Figure 9: Green LEDs' absorption at different water depth

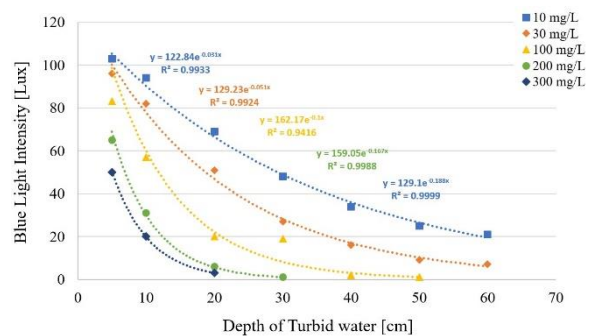


Figure 10: Blue LEDs' absorption at different water depth

of concentration 0, 10, 30, 100, 200, and 300 [mg/L] respectively. The solution is mixed in a 2L contained and poured into the PVC pipe. The test solution with 0 [mg/L] is the initial condition of the experiment where the light intensity data for each LED is considered maximum. This is because light is transmitted through clear tap water as such absorption from suspended matter is considered to insignificant. Due to the selected power LED (Figure 5) which has all the red, green and blue elements in one board, only one LED circuit is powered and the sensor data is stored then it is powered off before the next LED is powered and data is collected. The above steps are repeated for all selected water depths and concentration of Kaolin solution in order to validated the exponential relationship between the optical path and light intensity.

5.2. Results

The results of the experiment are presented in Figure 8, Figure 9 and Figure 10 showing the relationship between absorbed light intensity of red, green and blue LED light sources through different water depth and concentration of Kaolin solution respectively. From the data, it can be seen that the minimum coefficient of determination R^2 is 0.95, 0.98, and 0.97 for the Red, Green, and Blue respective light intensities. These high values validate the Bouguer-Beer-Lambert law which implies that for a distance z (Figure 2) between the light source and the light sensor, we can obtain the coefficient of absorption using Eq. 4. This goes to show that selecting a fixed optical path within 5 to 60 [cm] for our turbidity meter will yield reliable results for calculating the absorption coefficient. 10 [cm] is selected as the optical path for the turbidity meter. This is a 3D printed part called the Ambient Light Inhibitor as shown in Figure 4. This length is selected for 2 reasons;

- To conform with JIS which recommends 10 [cm] as maximum optical length when using the Kaolin standard for turbidity measurements.
- To maintain portability of the turbidity meter.

Having validated the high correlation between the optical path and light intensity in kaolin test solution, that the relationship is exponential in nature and fixed the path length, we conduct an experiment to determine the relationship between turbidity and the coefficient of absorption using the turbidity meter.

5.3. Experiment II

The aim of this experiment is to validate the wavelength dependent absorption coefficient using the turbidity meter. It is conducted within the same plastic container as specified in Table 2. No image data is required at this stage. Kaolin is incrementally dissolved in the water and data log of light reaching each light sensor is recorded. The concentrations of Kaolin are 0, 10, 100, 200, 300, and 400 mg/L.

The result of the data is plotted in Figure 11. The kaolin concentration at 0 mg/L is clear tap water which serves as the initial condition. The relationship is linear for the

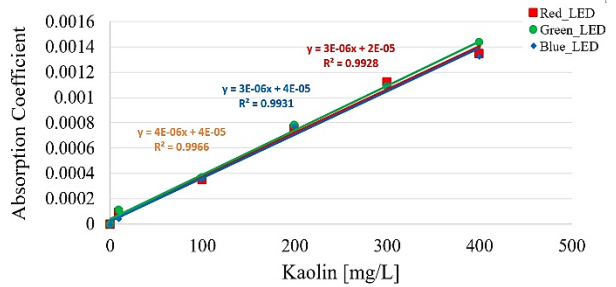


Figure 11: LED light absorption coefficient and turbidity

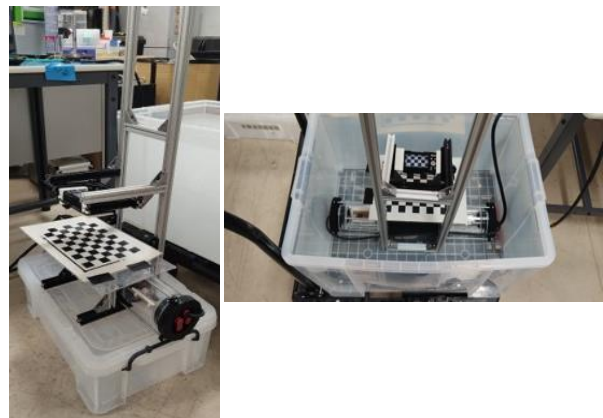


Figure 12: Experiment II setup: Left (Air) Right (clear)

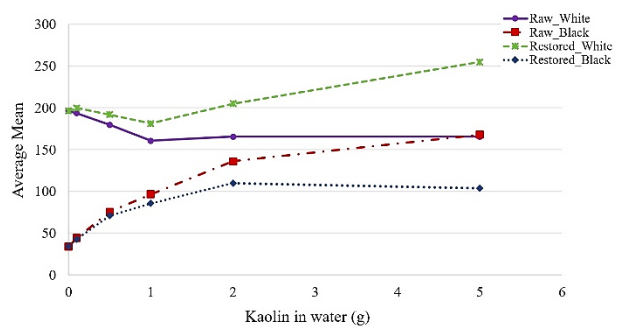


Figure 13: Average Mean values for raw and restored images

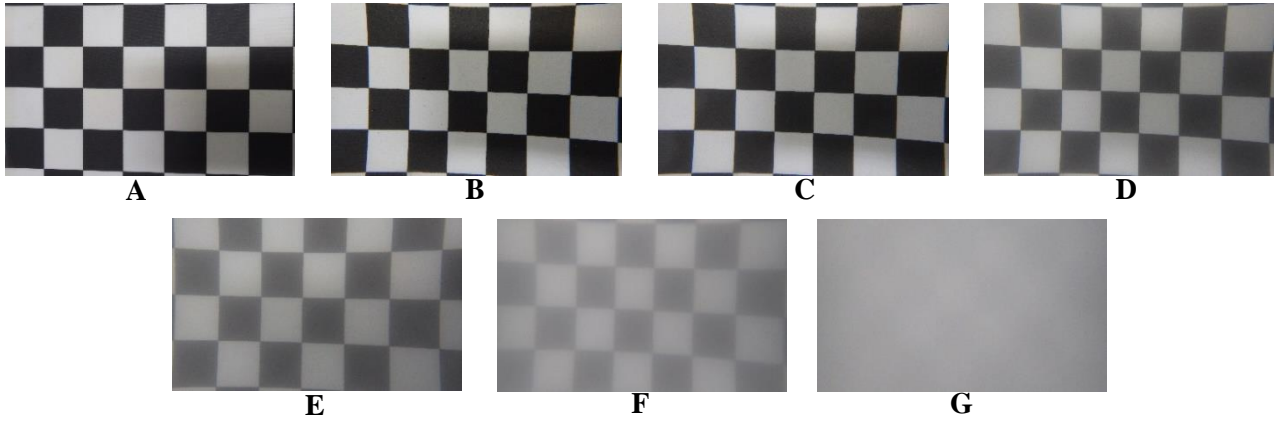


Figure 15: Raw images captured for different concentration of suspended particles.

(A = Air, B = 0g, C = 0.1g, D = 0.5g, E = 1g, F = 2g, G = 5g)

3 light sources which validates Eq. (4) being that the absorption coefficient has a proportional relationship to the concentration of kaolin with a strong coefficient of determination R^2 of 0.99 per light source.

However, the result is unclear if the absorption coefficient varies for different wavelengths because the data from 3 light sources all show very similar absorbance relationship. This could be attributed to a short optical path (10 cm) within which distinguishable information cannot be deduced. Perhaps if the optical path was long enough, information on which wavelength attenuates faster can be clearly seen. Attempting to resolve the challenge based on this is not feasible considering the portability requirement of the turbidity meter for ease of mounting on an AUV.

It might also be due to the selected light sensor (Figure 5) sensing the intensity of the light as a unit of LUX. From the datasheet, each LED emits light within a range of the visible region of the electromagnetic spectrum, although the dominant wavelength is given as the LED wavelength. Using a spectrometer for sensing the light might reveal more details on the range of wavelength

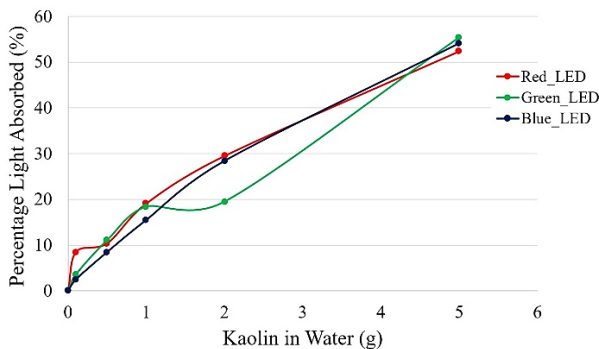


Figure 14: Percentage Absorption of light

that are attenuated more. This is a feasible solution that can be implemented as a next step in this research.

5.4. Experiment III

Table 2: Specification of items for experimentation

Item	Specification
PC	Windows, Arduino
Turbidity meter	
Power Supply	24V
Underwater Camera	RICOH WG-5
Checkerboard	Black/White
Plastic Container	660*390*440 (mm)
Tap water	70 (L)
Kaolin	0, 0.1, 0.5, 1, 2 & 5 (g)
Image Distance	200 (mm)

In this experiment, the kaolin standard is used to evaluate the effects of different concentration of suspended substances to underwater imaging. The aim is to restore the image to its original state using optical information from the turbidity meter. In doing so, images are captured in various underwater conditions while simultaneously recording the absorbance data for each of these conditions using the turbidity meter. The setup for the experiment is presented in Figure 12 and Table 2 shows the item specifications.

70L of clear tap water is placed in a plastic container. An image of a White/Black checkerboard is captured using a RICOH WG-5 underwater camera. The object-camera distance for the captured image is 200 (mm). The turbidity meter is immersed and data for the clear tap water is also captured and sent from Arduino to the PC. Both the image and turbidity data collected from the clear tap water serve as the initial condition data because the concentration of kaolin is 0g (in other words there are no suspended particles). This same procedure for capturing

image and turbidity data is repeated for 0.1, 0.5, 1, 2 and 5 [g] of kaolin is dissolved in the water. The water is intermittently stirred before and after adding kaolin to make a new solution. This is a precaution taken before collecting any data because kaolin particles are dense and tend to settle at the base of the plastic container.

Furthermore, instead of a colored checkerboard, a White/Black checkerboard is used as an initial step to form a basis for understanding the effects of the suspended particles on white and black pixels.

Finally, we limit the maximum concentration of kaolin to 5g because it is the point at which the threshold for distinguishing between the white and black pixels of the image is reached at this point. This can be seen from [Figure 15](#) where the raw images are shown.

5.5. Result discussion

This section discusses the results of analyzed image and turbidity data obtained from the experiment as well as the result of image restoration using the turbidity data. All the image processing procedure are carried out in MATLAB.

Image data analysis

From the image data obtained, it can be seen that increasing concentration of suspended particles affects both black and white pixels inversely (but not proportionally). From the raw images in [Figure 15](#), the black pixels begin to appear brighter while the white pixels, appear darker until they both reach a saturation point where both white and black pixels are the same.

To further validate the observed relationship; firstly, white and black regions of the raw images are cropped. Secondly, each of the cropped image are split into the RGB channels. The Mean of each channel is then calculated. The calculated channel-based Mean can be found in [Table 4](#). From the obtained Mean values, we observe that the degradation across the channels are very similar therefore, the average Mean value is calculated as shown in [Table 3](#). Using the average channel Mean value, [Figure 13](#) confirms the inverse effect of increasing suspended particles to white and black pixels. From the [Figure 13](#), the white pixel average Mean decreases with increasing suspended particles and quickly reach saturation at 1g of kaolin concentration while the black pixel average Mean increases continually till the 5g maximum of the experiment.

Turbidity meter data analysis

Using the Turbidity meter, the absorption of light intensity for each concentration of Kaolin is analyzed. The initial intensity of each LED (intensity recoded at 0g concentration of kaolin) is taken to be the maximum intensity that serve as a basis for subsequent steps in the restoration process. In the following steps, addition of Kaolin to the water reduced the intensity of light continually due to absorption from the suspended particles. In [Figure 14](#), a representation the relationship of percentage of absorbed light intensities to the Kaolin concentration. For better understanding of the relationship, the percentage absorbed intensity of each LED is calculated for each condition in the experiment and the result is depicted in the illustration. The Red LED is seen to have a higher rate of absorption when compared to the Green and Blue LEDs at the point where Kaolin concentration is increased by 0.1g from 0g. The Green LED on the other hand shows a steady increase in attenuation until the solution of 2g Kaolin where the percentage absorbed light reduces relative to the Red and Blue LEDs. However, the Blue LED shows even percentage absorption through all experiment concentration of Kaolin in water.

Analysis of Restored images

The analysis of the image restoration is based on the comparison with raw image data as shown in [Figure 13](#), [Table 3](#) and [Table 4](#). As earlier mentioned in [Section 3.1](#), the image restoration formulation used in this study is based on [Eq. 6](#) which restore the image based on the attenuated transmission signal. The backscattering component is not considered because of the limitation in the Turbidity meter design which measures channel based absorbed light only. However, because the effect of absorption affects the white and black pixels inversely, the attenuation coefficient is also inverted for each situation. That is to say, from [Eq. 2](#), the transmission is a function of $exp^{-\alpha_{\lambda}z(x)}$. The formula is used as such to restore white pixels, however for the black pixels, it reads as $exp^{\alpha_{\lambda}z(x)}$, the negative sign is removed in order to reverse the direction of restoration for the black pixels. [Table 4](#) presents a comparison of the cropped white and black pixel image before and after restoration. The cropped pixels taken in Air and 0g kaolin do not have corresponding restored images because they serve as the basis upon which all restored images are compared. This

means that all restored images should have RGB values that are close to the RGB values for the image taken at 0g kaolin solution. However, since a white/black checkerboard has been used, it is expected that the white and black pixels for the image take in Air and 0g kaolin should be close to or exactly 255 and 0 respectively. This is not the case as we can see from the Average Mean for white and black pixels in Air is 199.6 and 47.5, while that for the 0g image is 196.4 and 34 respectively. The is because of the fabric upon which the checkerboard is printed, it is not pure white and the black parts have faded over time and use. The lighting source might also be a factor that further affects the imaging.

Table 3: Average Mean for raw and restored images.

	Cropped White Region		Cropped Black Region	
	Raw Mean	Restored Mean	Raw Mean	Restored Mean
Air	199.6		47.5	
0	196.4		34	
0.1	193.6	199.7	44.2	42.8
0.5	179.7	191.9	75.5	70.7
1	160.6	181.2	96.4	85.4
2	165.5	204.9	136	109.8
5	165.4	254.9	167.9	103.8

We however make an initial observation from the image in Air and clear tap water. Generally, the image in water becomes darker than that in Air. This can be seen in [Table 4](#) where the channel Mean values for both white and black experience a slight reduction when in water as opposed to pixels in Air.

After restoration significant deviations take on restored white images for 0.1, 2 and 5 [g]. In the 0.1g image, the red channel Mean value surpasses that of the 0g and Air image although that of the green and blue channel improve proportionally, this disproportional increase in the red channel results in a pinkish-brown looking image. The reason for the disproportionate increase can be seen in [Figure 14](#) where the associated red LED percentage absorption is much higher than the blue and green absorption. This directly results in the over compensation of deteriorated red channel pixels of the restored image.

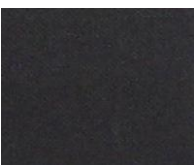
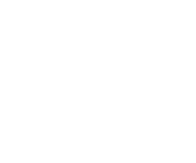
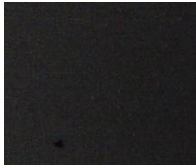
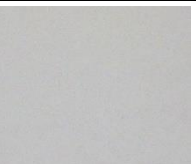
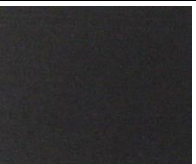
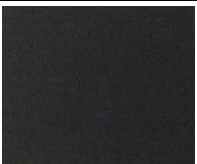
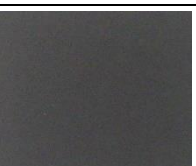
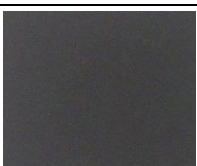
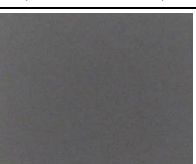
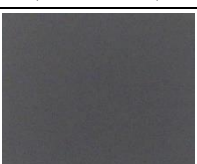
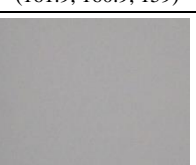
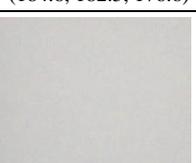
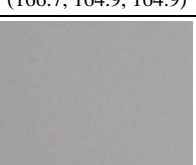
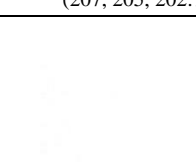
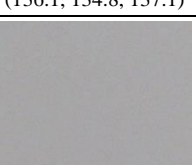
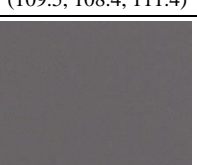
As for the 2g image, the RGB channel Mean all exceed marginally. However, the 5g image reaches the 255-maximum leading to a totally white image. It is unclear why the restoration at these levels exceed that of the 0g and Air images. Perhaps absorption information applied begins to have a negative correlation at higher degrees of turbidity in bright pixels.

For the restored black images, they are all restored within the range of the 0g/Air and the associated raw image channel Mean. There is no disproportionate channel Mean value in any of the images as in some of the restored whit pixels. The comparison can be seen in [Table 4](#).

6. Conclusion

In this paper, we describe the challenge of imaging in the underwater environment and propose to restore deteriorated underwater images using optical information of the underwater environment at the time of image capture. In doing so, a proposed optical sensing device; turbidity meter is designed and developed to measure light attenuation based on absorbed intensity of light transmitted over a predetermined optical path. Using the Kaolin standard, we conduct experiments to verify the relationship between the optical path and light intensity in varying concentration of kaolin standard solution. We also validated the Bouguer-Beer-Lambert law by experimenting with the turbidity meter and found a strong correlation between coefficient of absorption and concentration of kaolin. Finally, using the absorption data from the turbidity meter, deteriorated underwater images captured are restore using the attenuation component of the Image Formation Model. The results show some improvements for some images but the accuracy is low. To improve the results, we will modify the design of the turbidity meter to measure the backscattering in order to include the backscattering component of IFM. Also, a spectrometer sensor will be used to access wavelength specific information from the light source. There is also need to analyze a colored image before sea image trials.

Table 4: Tabulated comparison of raw images and restored images for cropped white and black regions of the checkerboard (Mean of the red, green and blue channel values for respective image)

Kaolin in Water (g)	Raw White pixel (Red, Green & Blue Mean)	Restored White pixel (Red, Green & Blue Mean)	Raw Black pixel (Red, Green & Blue Mean)	Restored black pixel (Red, Green & Blue Mean)
In Air	 (199.7, 199.3, 199.7)		 (47.2, 46.2, 49)	
0	 (197.3, 197.2, 194.6)		 (34.7, 33.6, 33.7)	
0.1	 (194.2, 193.8, 192.8)	 (205.2, 198.2, 195.8)	 (44.7, 43.5, 44.3)	 (42.4, 42.5, 43.4)
0.5	 (181, 180.5, 177.7)	 (193.9, 194.3, 187.7)	 (75.8, 75.1, 75.5)	 (70.7, 70, 71.5)
1	 (161.9, 160.9, 159)	 (184.6, 182.5, 176.6)	 (96.6, 95.7, 96.9)	 (84.7, 84.4, 87.2)
2	 (166.7, 164.9, 164.9)	 (207, 205, 202.7)	 (136.1, 134.8, 137.1)	 (109.5, 108.4, 111.4)
5	 (166.1, 164.5, 165.6)	 (254.8, 255, 255)	 (168.3, 166.9, 168.5)	 (106.2, 101.1, 104)

References

1. H. Blasinski and J. Farrell, "A three parameter underwater image formation model," *IS T Int. Symp. Electron. Imaging Sci. Technol.*, pp. 1–8, 2016, doi: 10.2352/ISSN.2470-1173.2016.18.DPMI-252
2. K. A. Skinner, J. Zhang, E. A. Olson, and M. Johnson-Roberson, "UWStereoNet: Unsupervised learning for depth estimation and color correction of underwater stereo imagery," *Proc. - IEEE Int. Conf. Robot. Autom.*, vol. 2019-May, pp. 7947–7954, 2019, doi: 10.1109/ICRA.2019.8794272.
3. J. Y. Chiang and Y. C. Chen, "Underwater image enhancement by wavelength compensation and dehazing," *IEEE Trans. Image Process.*, vol. 21, no. 4, pp. 1756–1769, 2012, doi: 10.1109/TIP.2011.2179666.
4. D. Berman, T. Treibitz, and S. Avidan, "Diving into haze-lines: Color restoration of underwater images," *Br. Mach. Vis. Conf. 2017, BMVC 2017*, pp. 1–12, 2017.
5. <https://global.ihs.com/standards.cfm?publisher=JSA>
6. E. McCartney, *Optics of the Atmosphere, Scattering by Molecules and Particles*, 1st ed., New York: John Wiley and Sons, 1976.
7. Qingsong Zhu; Jiaming Mai; Ling Shao, "A Fast Single Image Haze Removal Algorithm using Color Attenuation Prior," *IEEE Transactions on Image Processing*, vol. 24, no. 11, pp. 3522 - 3533, 2015.
8. N. G. Jerlov, *Marine Optics*, 2nd ed., Amsterdam, Holland: Elsevier Science Publishing Company, 2014, p. 231.
9. Derya Akkaynak; Tali Treibitz, "A Revised Underwater Image Formation Model," in *IEEE/CVF Conference on Computer Vision and Pattern Recognition*, Utah, USA, 2018.
10. D. Gillett and A. Marchiori, "A low-cost continuous turbidity monitor," *Sensors (Switzerland)*, vol. 19, no. 14, Jul. 2019, doi: 10.3390/s19143039.
11. L. C. Sperandio, M. S. Colombo, C. M. G. Andrade, and C. B. B. Costa, "Development of a low-cost portable turbidimeter for processes," May 2021, [Online]. Available: <http://arxiv.org/abs/2106.09491>.
12. C. D. Kelley *et al.*, "An affordable open-source turbidimeter," *Sensors (Switzerland)*, vol. 14, no. 4, pp. 7142–7155, Apr. 2014, doi: 10.3390/s140407142.
13. Y. Nishida, N. Sohara, S. Yasukawa, and K. Ishii, "Crack detection in a concrete structure using an underwater vehicle," *Proceedings of International Conference on Artificial Life and Robotics*, vol. 2021, pp. 777–781, 2021, doi: 10.5954/icarob.2021.os23-1.
14. N. Sohara, "Automatic Crack Detection of Underwater Infrastructure by Underwater Inspection Robot," Kitakyushu, Japan, 2020.
15. T. G. Mayerhöfer, S. Pahlow, and J. Popp, "The Bouguer-Beer-Lambert Law: Shining Light on the Obscure," *Chemphyschem*, vol. 21, no. 18, pp. 2029–2046, Sep. 2020,

doi: 10.1002/cphc.202000464.

Authors Introduction

Ms. Irimiya R. Inniyaka



He is a Master's degree holder in Automotive Mechatronics from the Department of Mechatronics, Cranfield University, in 2016. Currently he is conducting his Doctoral program at the Kyushu Institute of Technology, Japan. His research interests are in Underwater image processing and Generative Adversarial Networks.

Dr. Yuya Nishida



He is an Associate Professor at the Department of Human Intelligence Systems, Kyushu Institute of Technology, Japan. He obtained his Masters degree in Engineering in 2008 and his D. Eng. degree in 2011 at the same university. His research interests are in the field of Underwater Robotics, Field Robotics, and Intelligent Systems.

Prof. Kazuo Ishii



He a Professor at the Department of Human Intelligence Systems of Kyushu Institute of Technology, Japan. He obtained his M. S. degree in 1993 and his D. Eng. degree in 1996 at The University of Tokyo. His research interests are in the fields of Underwater Robotics, Field Robotics, Neural Networks and Intelligent Systems.
